Inorganic Chemistry

Article

pubs.acs.org/IC

Crystal Cluster Growth and Physical Properties of the $EuSbSe_3$ and $EuBiSe_3$ Phases

Scott Forbes,[†] Yu-Chih Tseng,[‡] and Yurij Mozharivskyj*[,†]

[†]Department of Chemistry and Chemical Biology, McMaster University, 1280 Main Street West, Hamilton, Ontario L8S 4M1, Canada

[‡]Canmet MATERIALS, National Resources Canada, 183 Longwood Road South, Hamilton, Ontario L8P 0A5, Canada

Supporting Information

ABSTRACT: Syntheses of europium metal, selenium powder, and the Sb_2Se_3/Bi_2Se_3 binaries were observed to produce crystal clusters of the $EuSbSe_3$ and $EuBiSe_3$ phases. These phases crystallize with the $P2_12_12_1$ space group and can be easily identified based on their growth habits, forming large clusters of needles. Previous literature suggested that their structure is charge-balanced with all europium atoms in the divalent state and one-quarter of the selenium atoms forming trimers. Physical property measurements on a pure sample of $EuSbSe_3$ revealed typical Arrhenius-type electrical resistivity, being approximately 3 orders of magnitude too large for thermoelectric applications. Electronic structure calculations indicated that both $EuSbSe_3$ and $EuBiSe_3$ are narrow-band-gap semiconductors, in good agreement with the electrical resistivity data. The valence and conduction band states near the Fermi level are dominated by the Sb/Bi and Se p states, as expected given their small difference in electronegativity.

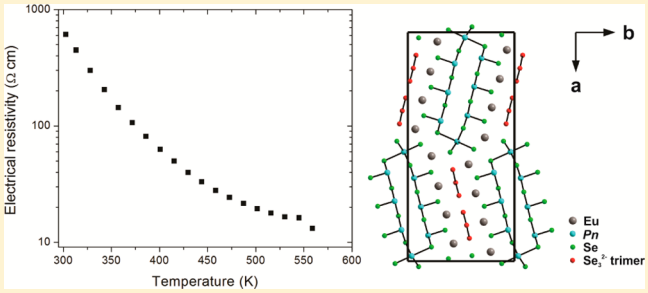

INTRODUCTION

Thermoelectric materials are able to perform two notable functions: they can act as power generators in the presence of a temperature gradient (Seebeck effect) and can be used for heating and cooling with the application of a current (Peltier effect).[1] The efficiency of a thermoelectric material (ZT) can be optimized with three ideal conditions: a high electrical conductivity, a high Seebeck coefficient, and a low thermal conductivity.[2] All three properties are themselves interrelated because the thermal conductivity of a sample partially depends on the conduction of charge carriers in a sample while a greater electrical conductivity, in turn, results in a lower Seebeck coefficient.[3] Narrow-band-gap semiconductors and semimetals are typically sought after because they have charge-carrier concentrations that yield optimized thermoelectric properties.[4] Many of the best thermoelectric materials known typically have maximum ZT values of 1.0−1.5 but can be nanostructured or mesostructured to obtain ZT values of around 2, previously seen in $AgPb_mSbTe_{2+m}$,[5] as well as in the Bi_2Te_3-[6] and PbTe-based[7] materials. However, in order for thermoelectric materials to be competitive with other energy sources for mainstream applications, a thermoelectric efficiency ZT of at least 4 is required, resulting in a Carnot efficiency of ∼30%.[8,9] Thus, while it is important to continue research in order to find ways to improve the physical properties of the current benchmark materials under study, it is also imperative that we continue to search for new and more efficient thermoelectrics.

One such material that caught our attention is the rather recently discovered $EuSbSe_3$ and $EuBiSe_3$ phases (Figure 1).[10]

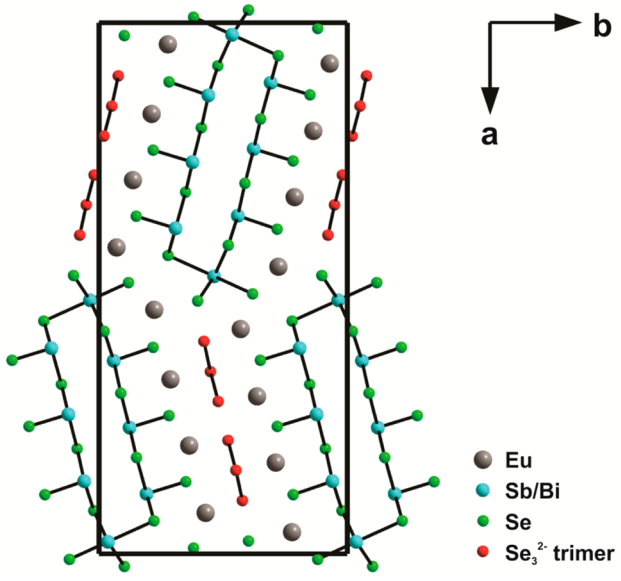

Figure 1. Eu(Sb/Bi)Se_3 structure, viewed along the *c* direction. Sb/Bi−Se slabs define the overall framework of the structure, with Eu^{2+} cations and Se_3^{2-} trimers occupying the spaces between the slabs.

Special Issue: To Honor the Memory of Prof. John D. Corbett

Received: August 6, 2014
Published: September 25, 2014

Both phases share the same structure type, previously reported for the $MPnSe_3$ series (M = Sr, Ba; Pn = Sb, Bi).[11,12] Their very large unit cells containing Sb/Bi−Se slabs and Se_3^{2-} trimers afford a high degree of complexity, which is quite attractive for potential thermoelectric use, particularly in reducing the thermal conductivity.[13] Covalency between Sb/Bi and Se is also beneficial because the weak bond order between these atoms will most likely yield a small separation in energy in bonding and antibonding states, a feature commonly associated with the values of electrical conductivity targeted for thermoelectrics. Our group has synthesized a set of $EuSbSe_3$ and $EuBiSe_3$ samples for physical property measurement. Their physical properties are presented and discussed in this work.

EXPERIMENTAL SECTION

Synthesis. All samples were made using high-purity europium metal (99.9 wt %, SmartElements), antimony metal (99.999 wt %, CERAC Inc.), bismuth metal (99.999 wt %, Alfa Aesar), and selenium shot (99.999 wt %, Alfa Aesar). The preparation of the $EuSbSe_3$ and $EuBiSe_3$ samples was performed in a manner similar to that outlined in the work by Albrecht-Schmitt and co-workers.[10] The Sb_2Se_3 and Bi_2Se_3 precursors were first prepared by heating the elements in a silica ampule at 800 °C for 24 h and then quenching in water. Carbon-coated silica tubes of roughly 20−25 cm length were used as ampules for all reactions performed. Carbon coating was accomplished by decomposition of acetone under a natural gas torch; this was done to avoid unwanted reactions between europium metal and silica at high temperatures. Each sample was added to a carbon-coated silica tube in a glovebox by combining europium metal filings, Sb_2Se_3/Bi_2Se_3 powder, and pulverized selenium powder in a 2:1:3 molar ratio, respectively. The samples were then evacuated to a pressure of roughly 10^{-5} Torr and were sealed using a torch. Shaking was performed to ensure a wide distribution of sample throughout the ampule; this matter is elaborated on further in the Results and Discussion section. Separate heating trends were used for the $EuSbSe_3$ and $EuBiSe_3$ samples, described in the precedent literature and summarized in Table 1. Upon reaction completion, long needlelike crystals were collected from each sample and often formed spherical-shaped or "bird's nest" clusters. Each sample was then analyzed and separated into different components using a tabletop microscope under 40× magnification. This was done to remove any obvious EuSe or molten Sb_2Se_3/Bi_2Se_3 impurities. Sufficiently pure isolated crystal clusters were then ground into a fine powder and pressed into 10 mm and $^1/_2$-in.-diameter pellets of roughly 2 mm thickness. These pellets were then sealed in silica ampules of roughly 10−15 cm length under 10^{-5} Torr vacuum. Annealing was performed at 325 °C for 3 days to ensure rigidity. The 10-mm-diameter pellet was then cut into a bar of roughly 8 × 2 × 2 mm dimensions for Seebeck and electrical resistivity tests, while the $^1/_2$-in. pellet was used for thermal diffusivity and specific heat capacity tests.

Table 1. Heating Trends Used To Form $EuSbSe_3$ and $EuBiSe_3$ Crystal Clusters

step	$EuSbSe_3$	$EuBiSe_3$
1	heat to 500 °C at 120 °C h^{-1}	heat to 600 °C at 120 °C h^{-1}
2	dwell for 1 h	dwell for 1 h
3	heat to 850 °C at 30 °C h^{-1}	heat to 900 °C at 30 °C h^{-1}
4	dwell for 144 h	dwell for 96 h
5	cool to 400 °C at 2.4 °C h^{-1}	cool to 500 °C at 1.8 °C h^{-1}
6	dwell for 48 h	dwell for 24 h
7	quench in water	quench in water

Single-Crystal X-ray Diffraction. Single crystals picked up from the samples were analyzed on a STOE IPDSII diffractometer using Mo Kα radiation in the whole reciprocal sphere. A numerical absorption correction was based on the crystal shape originally determined from optical face indexing but later optimized against equivalent reflections using the *STOE X-Shape* software.[14] Crystal structures were determined and solved using the *SHELX* software.[15] Both $EuSbSe_3$ and $EuBiSe_3$ adopt the orthorhombic $P2_12_12_1$ space group. The $EuSbSe_3$ crystal was refined to be a racemic mixture, while the $EuBiSe_3$ crystal was determined to only consist of one racemic component. Further information on the crystal structures can be found in the Supporting Information.

Powder X-ray Diffraction. Each sample was analyzed by powder X-ray diffraction on a PANalytical diffractometer using Cu Kα_1 incident radiation and an X'Celerator detector. Approximately 50 mg of the finely ground sample was deposited on a silicon zero-background sample holder coated with a thin layer of Vaseline. The diffraction data were collected in the 2θ range between 20° and 70° for all samples and analyzed using the Rietvald refinement method (*Rietica* program[16]) to determine sample purity and lattice constants. The structural parameters obtained from the single-crystal data[10] were used as starting models. The purity of each sample was then assessed based on the presence or absence of impurity peaks, as well as the refined weight percentages of each phase present.

Thermogravimetric Analysis (TGA) and Differential Thermal Analysis (DTA). TGA and DTA on all samples were performed using a Netzsch STA 409 PC/PG Luxx simultaneous thermal analyzer. Approximately 50 mg of sample was used for each data collection. All samples were contained within an aluminum oxide capsule and were heated at a rate of 5 K min^{-1} under an argon atmosphere. Aluminum oxide was used as a standard for calibration. Data collection was halted when a significant decrease in mass was observed in order to avoid instrument damage.

Thermoelectric Data. The Seebeck coefficient (S) and electrical resistivity (σ) data were measured in the temperature range from 25 to 300 °C in a ZEM series system (ZEM-3; ULVAC, USA) under a helium atmosphere. The thermal diffusivity was determined using the flash technique in a Netzsch laser flash measurement tool (LFA457).

Electronic Band Structure Calculations. The electronic structures of all samples for which a crystal could be obtained and solved were calculated using the tight-binding, linear-muffin tin orbital method[17] with the atomic sphere approximation (TB-LMTO-ASA), as implemented in the Stuttgart program.[18] All 4f electrons were considered as core electrons. Exchange and correlation were treated by the local density approximation.[19] A scalar relativistic approximation[20] was employed to account for all relativistic effects except spin−orbit coupling. Overlapping Wigner-Seitz cells were constructed with radii determined by requiring the overlapping potential to be the best approximation to the full potential, according to the atomic sphere approximation (ASA). Automatic sphere generation[21] was performed to construct empty spheres to be included in the unit cell in order to satisfy the overlap criteria of the TB-LMTO-ASA model. The single-crystal X-ray data from the original publication,[10] including lattice parameters and atomic coordinates, were used as the models for calculations.

RESULTS AND DISCUSSION

Formation and Purity of $EuSbSe_3$ and $EuBiSe_3$. All reactions performed in this study typically result in a mixture of $EuSbSe_3/EuBiSe_3$ as the majority phase, with EuSe and Sb_2Se_3/Bi_2Se_3 as the minor phases. It was noticed that in most cases, upon analysis by powder X-ray diffraction and Rietvald refinement, the purity of each sample will normally be around 75% for the $EuSbSe_3$ samples and below 50% for the $EuBiSe_3$ samples. As such, the products obtained from each reaction had to be separated under a tabletop microscope into their respective components. This is quite possible because the $EuSbSe_3$ and $EuBiSe_3$ phases typically form very distinct spherical and "bird"s nest" crystal clusters composed of long black needles of up to 2 cm length (Figure 2). The Sb_2Se_3/Bi_2Se_3 impurities can also be easily identified based on their molten, rocklike appearance, although the $EuSbSe_3/EuBiSe_3$

dx.doi.org/10.1021/ic501808y | *Inorg. Chem.* 2015, 54, 815−820

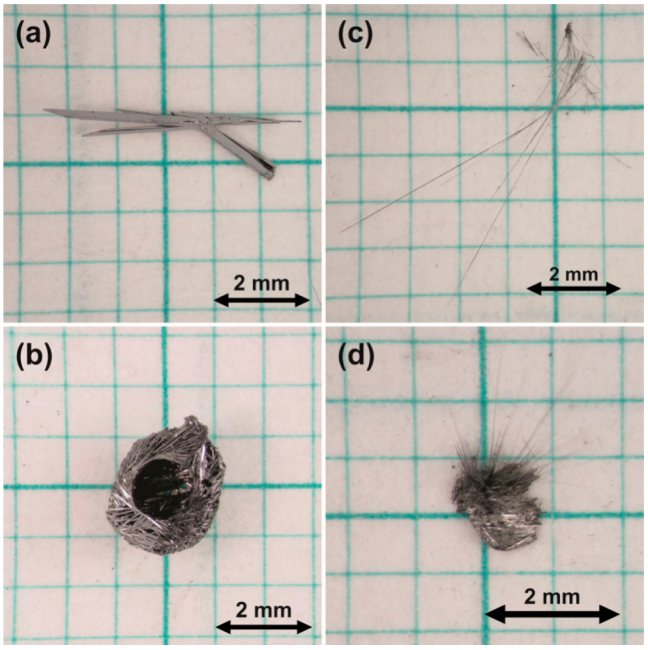

Figure 2. Needlelike crystals and crystal clusters of the $EuSbSe_3$ phase (a and b) and the $EuBiSe_3$ phase (c and d). The $EuSbSe_3$ phase typically forms spherical and "bird's nest" clusters, while the $EuBiSe_3$ phase forms smaller, irregularly shaped clusters.

phases can typically be found in respectable amounts in these components as well. The EuSe impurities are difficult to detect by eye because EuSe remains solid even at the highest temperature used in the heating trend (melting point of 2215 °C) and does not crystallize in any obvious motif. It is likely that any EuSe that forms by this method either is in powder form or is incorporated into the crystal clusters that are isolated from the entire batch because even the most pristine clusters washed and dried with acetone typically contain at least 1−3% EuSe by weight. This incorporation into the highly unusual "bird's nest" $EuSbSe_3$ crystal clusters may be possible if a solid piece of EuSe acts as a nucleation center, yielding the small amount of impurity seen in refinement.

Despite the slow cooling and long heat treatments, it is nearly impossible to completely avoid the formation of impurities and/or decomposition of the products. TGA confirmed that the $EuSbSe_3$ phase is stable up to approximately 400 °C, after which sharp mass losses are observed. DTA did not yield any significant features such as structural transitions or phase changes in the measured region. A sample of $EuSbSe_3$ sealed in a silica ampule and heated in a box furnace at 350 °C for 3 days had a powder X-ray diffraction pattern with no obvious change in the impurity concentration. However, a sample heated at 500 °C for 3 days was found to have significant decomposition, mostly resulting in Sb_2Se_3 and EuSe impurities (any remaining europium metal would likely have reacted with the silica). The most obvious way to avoid the formation or remnants of the Sb_2Se_3/Bi_2Se_3 impurities would be to substitute them for elemental antimony/bismuth and selenium, although this was determined to yield only trace amounts of the desired phases. The EuSe impurity is also difficult to avoid, given that the loading composition includes both europium metal and selenium powder, and EuSe is both extremely stable[22] and structurally simplistic. A separate experiment was performed in which the Sb_2Se_3/Bi_2Se_3 and selenium powder portions of the samples were pressed into a pellet and physically separated from the europium metal on different sides of the ampule. Surprisingly, this method did not appear to make any significant difference in the quality of each sample because EuSe was still observed to form. This can be explained by the nature of the sample formation itself, which requires an initial high temperature to induce a relatively high partial pressure of all three species present in the ampule. The components then react in the vapor phase and deposit the crystals and crystal clusters on the sides of the silica ampule rather than just on the bottom. Because these components are in the vapor phase, a competing reaction between the formation of EuSe and $EuSbSe_3/EuBiSe_3$ occurs; the formation of $EuSbSe_3$ is strongly preferred, with $EuBiSe_3$ forming in modest amounts. This method of reaction is further supported by a separate set of experiments in which all three reaction species were mixed together, pressed into pellets, and heated by the same heating trends as those outlined in Table 1. Only trace amounts of $EuSbSe_3$ and $EuBiSe_3$ were observed, with the major products being Sb_2Se_3/Bi_2Se_3 and EuSe.

The existence of $EuSbSe_3$ and $EuBiSe_3$ may also suggest that other related phases exist, such as the divalent ytterbium analogues or the corresponding tellurides, given the similar nature between selenium and tellurium. We attempted to produce these phases for each combination of $(Eu/Yb)(Sb/Bi)(Se/Te)_3$, but only the $EuSbSe_3$ and $EuBiSe_3$ samples yielded crystals, while all other samples yield only binary phases. It is likely that Yb^{2+} cannot be stabilized by this structure because Yb^{2+} is more reducing[23] compared to Eu^{2+} and cannot possibly support the existence of trimeric selenium or tellurium. The $EuSbTe_3$ and $EuBiTe_3$ analogues may not exist either because of the greater instability of tellurium trimers (Te_3^{2-}) with respect to selenium trimers (Se_3^{2-})[24] or because of improper reaction conditions. While it is true that we used only two heating trends, one for antimony-containing samples and one for bismuth-containing samples, each sample was heated to temperatures great enough to induce a vapor-phase reaction for all species present; thus, we do not believe that any of the aforementioned analogues exist.

By our experimental procedure, a mass yield of roughly 40−50% of a pure batch of the $EuSbSe_3$ phase could be obtained with consistency. It was noticed, however, that a slight change of the heating trend used produced very different results; even using two different furnaces resulted in a significant purity difference in identically prepared samples. While the $EuSbSe_3$ phase could reliably be prepared and isolated, the results were quite different for $EuBiSe_3$. It was noticed in all experiments that not only does $EuBiSe_3$ form in much smaller yields than the $EuSbSe_3$ phase, but it is also nearly impossible to separate it from the impurities present, resulting in purities of no better than 70%. This is most notably the result of poor crystal cluster growth, as one can see from Figure 1; the $EuBiSe_3$ needle clusters are much smaller than their $EuSbSe_3$ counterparts and rarely form any of the same spherical or "bird's nest" shapes. This is possibly due to the heating trend used, which may be far from optimized for promoting the growth of these clusters. If one were to produce larger clusters of crystals that could be easily separated from impurities, a different heating trend must be used. As a result of the low purity of the $EuBiSe_3$ samples, we were unable to prepare a sample for physical property measurement.

Physical Properties of $EuSbSe_3$. As mentioned in the Introduction, both $EuSbSe_3$ and $EuBiSe_3$ are expected to be

dx.doi.org/10.1021/ic501808y | Inorg. Chem. 2015, 54, 815−820

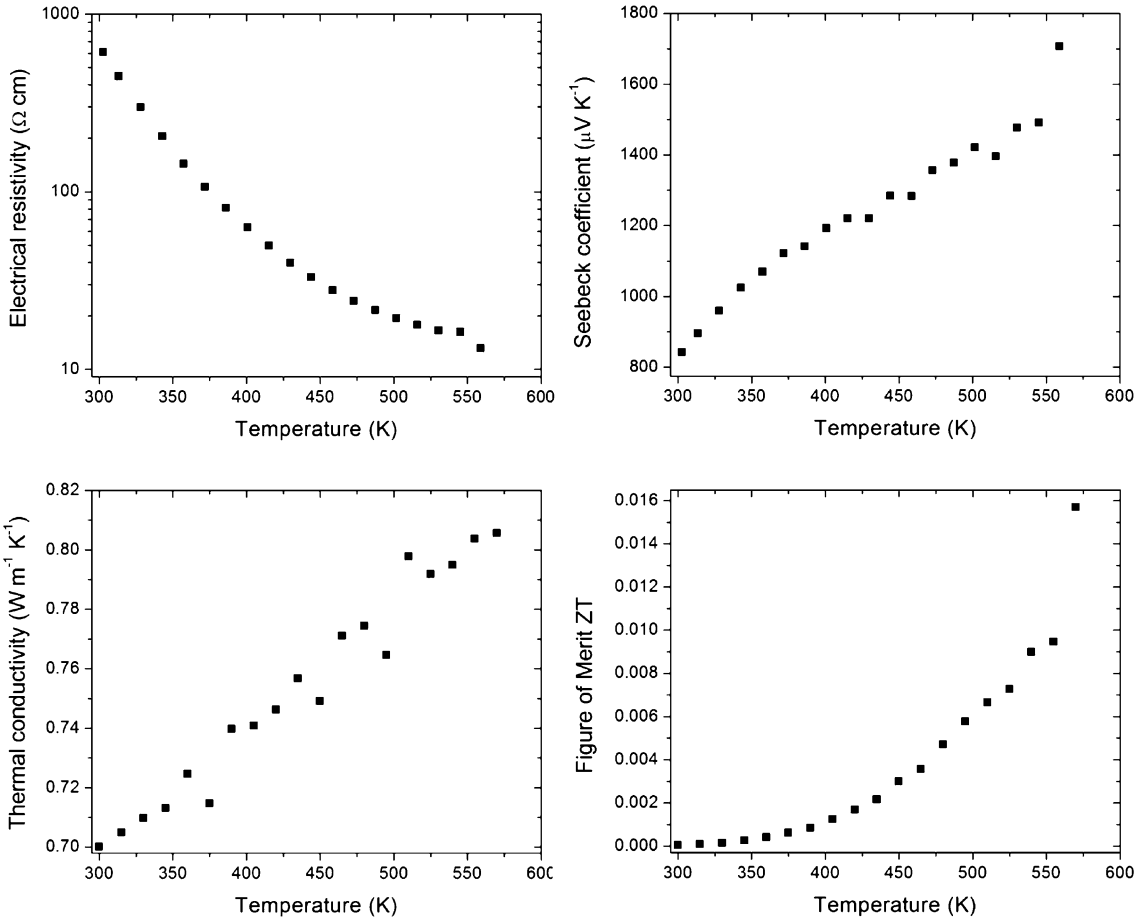

Figure 3. Electrical resistivity (top left), Seebeck coefficient (top right), thermal conductivity (bottom left), and thermoelectric efficiency (bottom right) versus temperature of a $EuSbSe_3$ sample.

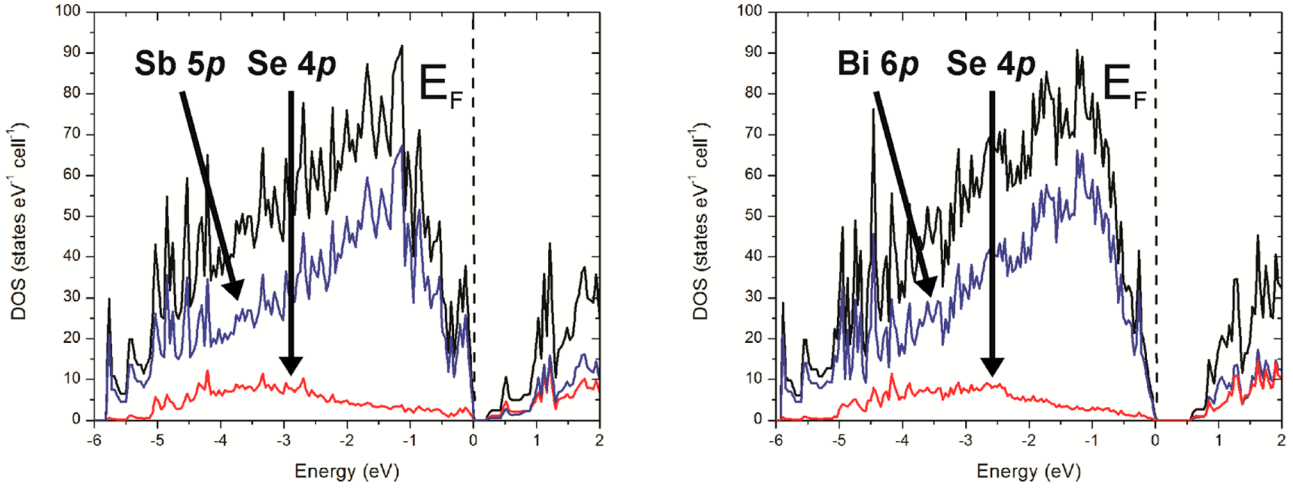

Figure 4. Calculated electronic structures of the $EuSbSe_3$ (left) and $EuBiSe_3$ (right) phases. The total DOS (black) and element DOS (red and blue) represent the bonding character of each structure.

semiconductors given the divalent nature of europium, as confirmed by magnetic measurements and the formation of selenium trimers (Se_3^{2-}), resulting in a charge-balanced $(Eu^{2+})_4(Pn^{3+})_4(Se_3^{2-})(Se^{2-})_9$ formula.[10] Physical property measurements on a sample of $EuSbSe_3$ revealed an exponential decrease in the electrical resistivity along with a steady increase in the Seebeck coefficient (Figure 3), behavior typically associated with nondegenerate semiconductors and in support of the charge-balanced model. The $EuSbSe_3$ data were fitted to the Arrhenius equation, which yielded an activation energy of 0.25(3) eV. As a precaution, we did not measure any properties above approximately 560 K because sample decomposition may lead to the release of selenium or selenium-containing impurities that could contaminate and/or damage the instruments. While the thermoelectric properties would likely be somewhat improved at higher temperatures, the relatively small

dx.doi.org/10.1021/ic501808y | Inorg. Chem. 2015, 54, 815−820

activation energy implies that a maximum in the Seebeck coefficient would soon be reached because both charge-carrier types would be promoted across the band gap. Furthermore, the minimum electrical resistivity attains a value of approximately 10 Ω cm, which is at least 3 orders of magnitude too great for any realistic thermoelectric applications. On the basis of the exponential trend of the data, it would not be possible to achieve the desired value for the electrical conductivity in the stability range of the structure.

Thermal conductivity measurements performed on a sample of the $EuSbSe_3$ phase yielded very low values ranging from 0.7 to 0.8 W m^{-1} K^{-1} (Figure 3), although this is primarily due to both the porosity of the sample (a measured density of 4.81 g cm^{-3} versus the theoretical density of 6.28 g cm^{-3}) and the low contribution of the electronic thermal conductivity according to the Wiedemann–Franz law. Thus, the thermal conductivity of $EuSbSe_3$ corresponds almost exclusively to the lattice thermal conductivity. The sample was observed to experience a slight increase in the thermal conductivity with increasing temperature, which is not uncommon (Bi_2Te_3 displays a continuous increase in the thermal conductivity in its operational range[25]). The behavior of the data obtained is somewhat erratic and originates from the specific heat capacity of the sample, which fluctuates slightly as a result of potential selenium losses or local density changes due to the sample porosity. The thermoelectric figure of merit of the $EuSbSe_3$ phase is far from desirable, reaching a maximum ZT of about 0.016 at 560 K. We therefore conclude that $EuSbSe_3$ does not have any potential use for thermoelectric applications.

Electronic Structures of $EuSbSe_3$ and $EuBiSe_3$. The calculated electronic structures of both phases indicate the presence of a band gap at the Fermi level (Figure 4), which agrees with the charge-balanced $(Eu^{2+})_4(Pn^{3+})_4(Se_3^{2-})(Se^{2-})_9$ formula and the Arrhenius-type electrical resistivity behavior of the $EuSbSe_3$ sample. While we were unable to measure the electrical resistivity of the $EuBiSe_3$ phase, given its similarity to $EuSbSe_3$, it is likely that it will also behave as a semiconductor. Interestingly, both phases display a very large density of states (DOS) near the Fermi level in the valence band, with a very sharp slope near the zero energy. This may be of interest, given the fact that a small change in energy accompanied by a large change in the DOS ($\partial DOS/\partial E$) results in a large increase in the Seebeck coefficient with little to no effect on the electrical resistivity, resulting in a decoupling of the thermoelectric properties.[26,27] This feature can be quite attractive for thermoelectric applications because it allows for the simultaneous optimization of both properties and a large improvement in the figure of merit. It is unlikely that the $EuBiSe_3$ structure would display significantly better thermoelectric properties compared to $EuSbSe_3$ because its calculated band gap is nearly twice as large. Furthermore, an antimony–chalcogenide framework is known to yield better electrical conductivity than an isostructural bismuth–chalcogenide framework, as is the case with Sb_2Te_3 versus Bi_2Te_3.[28,29] However, if $EuBiSe_3$ could be prepared and isolated in high purity in appreciable amounts, it would still be worth investigating as a comparison to $EuSbSe_3$.

Both electronic structures were analyzed for the contributions to the total DOS for each set of atoms. Our calculations revealed that the europium atoms do not significantly contribute to the states near the Fermi level. It was determined that the valence band states near the Fermi level were primarily composed of Se p states, while the states in the conduction band near the Fermi level were dominated by a nearly even contribution of antibonding selenium trimer (Se_3^{2-}) and Sb/Bi p states. This is not surprising because the charge-balanced $(Eu^{2+})_4(Pn^{3+})_4(Se_3^{2-})(Se^{2-})_9$ formula would indicate that the selenium orbitals are mostly occupied (partial occupancy for the Se_3^{2-} groups) and the Sb/Bi p states are both empty and slightly higher in energy because of the more electronegative nature of selenium compared to antimony and bismuth. As mentioned earlier, the electronic band gap for $EuBiSe_3$ is nearly twice as large at the band gap for $EuSbSe_3$. This can be rationalized by the larger electronegativity difference between bismuth and selenium compared to antimony and selenium (in Pauling units: 1.82 for antimony, 1.67 for bismuth, and 2.48 for selenium),[30] which results in a greater separation in energy between the bonding and antibonding states in the $EuBiSe_3$ structure. Thus, the band gap and electrical conductivity of the sample can be effectively tuned by the substitution of antimony and bismuth with each other or by the substitution of selenium with another element such as tellurium, if possible.

CONCLUSIONS

Synthesis of the $EuSbSe_3$ and $EuBiSe_3$ phases was motivated by our efforts to discover new and more efficient thermoelectric materials. Both phases contain great structural complexity, heavy elements, and were predicted to be semiconducting. Synthetic conditions determined from previous literature were used to form crystal clusters of both phases, although only the $EuSbSe_3$ phase could be reliably produced in bulk quantities and separated from impurities.

Physical property tests confirmed that $EuSbSe_3$ will remain stable up to approximately 400 °C, above which it decomposes into primarily EuSe and Sb_2Se_3. Electrical resistivity measurements on a sample of $EuSbSe_3$ yielded the lowest values of roughly 10 Ω cm, which is too high for any potential thermoelectric use. While the Seebeck coefficient and thermal conductivity values are both attractive, the maximum thermoelectric figure of merit of 0.016 achieved at 560 K dismisses any potential thermoelectric applications for $EuSbSe_3$. The $EuBiSe_3$ phase, while potentially displaying interesting physical properties, requires a different heating trend to yield a greater quantity of crystals before it can be tested for physical properties.

ASSOCIATED CONTENT

Supporting Information

Single-crystal X-ray data of $EuSbSe_3$ and $EuBiSe_3$ crystals, including refinement parameters and atomic coordinates, and X-ray crystallographic data in CIF format. This material is available free of charge via the Internet at http://pubs.acs.org.

AUTHOR INFORMATION

Corresponding Author

*E-mail: mozhar@mcmaster.ca.

Notes

The authors declare no competing financial interest.

ACKNOWLEDGMENTS

This work was supported by Discovery and CREATE HEATER grants from the Natural Sciences and Engineering Research Council of Canada. The authors would like to acknowledge the support of the Resource for the Innovation of Engineered Materials program at CanmetMATERIALS of Natural Resources Canada.

REFERENCES

(1) Tritt, T. M. *Science (Washington, D.C.)* **1996**, *272*, 1276−1277.
(2) Snyder, G. J.; Toberer, E. S. *Nat. Mater.* **2008**, *7*, 105−114.
(3) Sootsman, J. R.; Chung, D. Y.; Kanatzidis, M. G. *Angew. Chem., Int. Ed.* **2009**, *48*, 8616−8639.
(4) Mahan, G.; Sales, B.; Sharp, J. *Phys. Today* **1997**, *50*, 42−47.
(5) Hsu, K. F.; Loo, S.; Guo, F.; Chen, W.; Dyck, J. S.; Uher, C.; Hogan, T.; Polychroniadis, E. K.; Kanatzidis, M. G. *Science (Washington, D.C.)* **2004**, *303*, 818−821.
(6) Polvani, D. A.; Meng, J. F.; Shekar, N. V. C.; Sharp, J.; Badding, J. V. *Chem. Mater.* **2001**, *13*, 2068−2071.
(7) Biswas, K.; He, J.; Blum, I. D.; Wu, C.-I.; Hogan, T. P.; Seidman, D. N.; Dravid, V. P.; Kanatzidis, M. G. *Nature (London, U.K.)* **2012**, *489*, 414−418.
(8) Disalvo, F. J. *Science (Washington, D.C.)* **1999**, *285*, 703−706.
(9) Tritt, T. M. *Science (Washington, D.C.)* **1999**, *283*, 804−805.
(10) Bang Jin, G.; Crerar, S. J.; Mar, A.; Albrecht-Schmitt, T. E. *J. Solid State Chem.* **2006**, *179*, 1596−1601.
(11) Cook, R.; Schaefer, H. *Rev. Chim. Miner.* **1982**, *19*, 19−27.
(12) Cook, R.; Schaefer, H. *Stud. Inorg. Chem.* **1983**, *3* (Solid State Chem.), 757−60.
(13) Slack, G. A. In *CRC Handbook of Thermoelectrics*; Rowe, D. M., Ed.; CRC Press: Boca Raton, FL, 1995.
(14) *STOE X-Shape*; STOE & Cie GmbH: Darmstadt, Germany, 2004.
(15) Sheldrick, G. M. *SHELXL*; University of Gottingen: Gottingen, Germany, 1997.
(16) Hunter, B. *Rietica*; Australian Nuclear Science and Technology Organization: Menai, Australia, 2000.
(17) Andersen, O. K.; Pawlowska, Z.; Jepsen, O. *Phys. Rev. B: Condens. Matter Mater. Phys.* **1986**, *34*, 5253−69.
(18) Jepsen, O.; Burkhardt, A.; Andersen, O. K. *TB-LMTO-ASA Program*, version 4.7; Max-Planck-Institut für Festkörperforschung: Stuttgart, Germany, 1999.
(19) Andersen, O. K.; Jepsen, O. *Phys. Rev. Lett.* **1984**, *53*, 2571−2574.
(20) Andersen, O. K.; Jepsen, O.; Glotzel, D. In *Highlights of Condensed Matter Theory*; Bassani, F., Fumi, F., Tosi, M. P., Eds.; Elsevier: Amsterdam, The Netherlands, 1985.
(21) Jepsen, O.; Andersen, O. K. *Phys. B.: Condens. Matter* **1995**, *97*, 35−47.
(22) Reed, T. B.; Fahey, R. E.; Strauss, A. J. *J. Cryst. Growth* **1972**, *15*, 174−8.
(23) Morss, L. R. *Chem. Rev.* **1976**, *76*, 827−42.
(24) Balasubramanian, K.; Dai, D. *J. Chem. Phys.* **1993**, *99*, 5239−50.
(25) Poudel, B.; Hao, Q.; Ma, Y.; Lan, Y.; Minnich, A.; Yu, B.; Yan, X.; Wang, D.; Muto, A.; Vashaee, D.; Chen, X.; Liu, J.; Dresselhaus, M. S.; Chen, G.; Ren, Z. *Science (Washington, D.C.)* **2008**, *320*, 634−638.
(26) Heremans, J. P.; Jovovic, V.; Toberer, E. S.; Saramat, A.; Kurosaki, K.; Charoenphakdee, A.; Yamanaka, S.; Snyder, G. J. *Science (Washington, D.C.)* **2008**, *321*, 554−557.
(27) Mahan, G. D.; Sofo, J. O. *Proc. Natl. Acad. Sci. U. S. A.* **1996**, *93*, 7436−7439.
(28) Harman, T. C.; Paris, B.; Miller, S. E.; Goering, H. L. *Phys. Chem. Solids* **1957**, *2*, 181−90.
(29) Yang, J.; Aizawa, T.; Yamamoto, A.; Ohta, T. *J. Alloys Compd.* **2000**, *309*, 225−228.
(30) Allred, A. L.; Rochow, E. G. *J. Inorg. Nucl. Chem.* **1958**, *5*, 264−8.